

The generalised proximity effect model in superconducting bi- and trilayer films

G. Brammertz¹, A. Poelaert¹, A. Golubov², P. Verhoeve¹,
A. Peacock¹, H. Rogalla².

¹*Astrophysics Division, Space Science Department,
European Space Agency, ESTEC,
Noordwijk, The Netherlands*

²*Faculty of Applied Physics, Low Temperature Group,
University of Twente,
Enschede, The Netherlands*

August 28, 2018

Abstract

This paper presents a general model for calculating the density of states and the Cooper pair potential in proximised superconducting bi- and trilayer films. It is valid for any kind of bilayer S_1 - S_2 , whatever the quality of the materials S_1 and S_2 , the quality of the S_1 - S_2 interface and the layer thicknesses. The trilayer model is valid for a thin S_3 layer, whereas the other two layers have arbitrary thicknesses. Although the equations of the dirty limit are used, it is argued that the model stays valid in clean bi- and trilayer films. The typical example of superconducting tunnel junctions is used to show that existing models, applying to very thin or very thick layers, or to perfectly transparent S_1 - S_2 interfaces, are too restrictive to apply to any bilayer. The new model is applied to existing junctions, with layer thicknesses intermediate between the 'thick' and the 'thin' approximation.

I INTRODUCTION

Understanding the proximity effect in superconducting films is important for the development of practical devices such as superconducting tunnel junctions (STJ's). Depositing a superconductor S_1 onto another S_2 modifies the properties of both S_1 and S_2 materials. If both superconductors are thick enough (typically thicker than $10 \xi_{S_1(S_2)}$, with $\xi_{S_1(S_2)}$ the coherence length of S_1 (S_2)), the extremities of the bilayer behave as bulk materials obeying the BCS theory, though not necessarily like bulk S_1 and bulk S_2 . The intermediate region around the S_1 - S_2 interface is characterised by a relatively sharp transition between the two bulk-like regions, and can be pretty far from a BCS-like description. If the layers are relatively thin, any BCS-like behaviour can be absent from the structure. Finally, in the case where the layers are extremely thin, as described by McMillan [1], each layer behaves again like a BCS superconductor.

The physical quantities affected in a proximised bulk superconductor, are the Cooper pair potential Δ , the density of states for the Cooper pairs, P , and the density of states for the quasiparticles, N . As the density of states in both superconductors is modified due to the proximity effect, the resultant bandgap Δ_g lies at an intermediate value between the bulk values for S_1 and S_2 , Δ_{g,S_1} and Δ_{g,S_2} respectively. This feature has been fully described in the specific case, of a thin, low bandgap material S_2 next to a thick, high bandgap material S_1 , with both superconductors in the dirty limit [2, 3].

The goal of the present paper is to present the need for, and develop a model of, the proximity effect, which is not restricted to this very specific case.

In particular section V shows that there are many situations where this special case does not apply, and for which the simple BCS approach does not provide a satisfactory description. Specifically, in the case of STJ's used as photon detectors, a more general description of the proximity effect is required to adequately address such issues as device performance.

The general conditions for an extended model are presented in Section III. Such a model can be applied not only to STJ's, but also to any application involving bi- or trilayers of superconductors. The single factor which would make the model inapplicable is the roughness

of the S_1 - S_2 interface. The limitations caused by this parameter are therefore also discussed.

The extended model is described in Section II, while numerical calculations based on the model are presented in Section IV. The model is applied to existing STJ's in Section V, so as to highlight a typical application of the model.

II The generalised proximity effect model

The proximity effect in dirty S_1 - S_2 bilayers was studied previously in [3], [4]-[6] for the case of arbitrary transparency of the S_1 - S_2 interface, but only the case of a thin S_2 layer and bulk S_1 layer was considered. More recently, the case of arbitrary thickness of S_2 and S_1 layers was considered in [6], but only the limiting case of the high transparency of the S_1 - S_2 interface with $T_{c,S_2} = 0$ was studied. Here we generalise the theory to the case of arbitrary S_2 and S_1 layer thicknesses for the most general case of a finite critical temperature for the S_2 layer with $T_{c,S_2} < T_{c,S_1}$. We also consider the case of trilayer systems $S_1 - S_2 - S_3$ with a very thin S_3 layer. The trilayer model remains valid for any thickness of S_1 and S_2 . The model is constructed for the case of $T_{c,S_3} < T_{c,S_1}$, but T_{c,S_2} can have any value.

In case where the relevant length scales (coherence lengths, mean free paths and sample thicknesses) are much larger than the atomic scale, the proximity effect can be described in terms of a quasiclassical Green's function formalism [7]-[11].

For an arbitrary relationship between the electronic mean free path and the coherence length the density of states can be derived from the solution of the Eilenberger equations [8]. If the vector potential is zero the Eilenberger equations have the form

$$\mathbf{v}_F \frac{\partial}{\partial \mathbf{r}} \hat{g}(\omega_n, \mathbf{r}) + \left[\omega_n \hat{\sigma}_3 - \Delta(\mathbf{r}) \hat{\sigma}_1 - \frac{1}{\tau} \langle \hat{g}(\omega_n, \mathbf{r}) \rangle, \hat{g}(\omega_n, \mathbf{r}) \right] = 0. \quad (1)$$

In this expression, \mathbf{v}_F is the Fermi velocity, $\hat{g} = \hat{\sigma}_3 g + \hat{\sigma}_1 f$ is the matrix Green's function, Δ is the Cooper pair potential, τ is the scattering time of the quasiparticles, and $\hat{\sigma}_i$ are Pauli matrices. The energy is quantified by the Matsubara frequency, given by $\omega_n = \pi T(2n + 1)$ (T is the temperature); the available energies ϵ for the quasiparticles are related to the Matsubara

frequencies by the relation $\omega_n = -i\epsilon$. The brackets $\langle \dots \rangle$ denote an averaging over the Fermi surface. In the dirty limit, the scattering centres ensure that the Green's functions are isotropic all through the sample. This fact allows Eq. (1) to be simplified into a diffusion equation for a Green's function $\widehat{G}(\omega_n, r)$, which is independent of the angles of the vector \mathbf{v}_F . In this case the function \widehat{g} may be represented by the form [11]

$$\widehat{g}(\omega_n, \mathbf{r}) = \widehat{G}(\omega_n, r) + \mathbf{n}\widehat{G}_1(\omega_n, r), \quad \widehat{G}_1 \ll \widehat{G}, \quad (2)$$

\mathbf{n} being the unit vector in the direction of the momentum of the quasiparticles.

It can be shown that $\widehat{G}_1 = \mathbf{v}_F \tau \widehat{G} \frac{\partial}{\partial \mathbf{r}} \widehat{G}$ [9, 11]. In the case of a short mean free path, the quantity $\mathbf{v}_F \tau$ is small, and the condition $\widehat{G}_1 \ll \widehat{G}$ which is required in Equation (2) is satisfied. This is the condition which is realised either in the case of a high concentration of impurities in a bulk superconductor or dislocation scattering centres, or in the case of strong diffusive boundary scattering in a film.

We consider a superconducting film S_i in which the dirty limit condition $l_{S_i} \leq \xi_{S_i}$ is fulfilled. Here l_{S_i} is the electronic mean free path. The coherence length ξ_{S_i} is related to the diffusion coefficient D_{S_i} by the relation $\xi_{S_i} = \sqrt{D_{S_i}/2\pi T_{c,S_i}}$. We shall define the x axis as perpendicular to the film surface. The Usadel equations [9], directly derived from Eq.1 can be written as

$$\xi_{S_i}^2 \theta_{S_i}''(x) + i\epsilon \sin \theta_{S_i}(x) + \Delta_{S_i}(x) \cos \theta_{S_i}(x) = 0 \quad (3)$$

where the pair potential Δ_{S_i} is determined by the self-consistency relation

$$\Delta_{S_i}(x) \ln \frac{T}{T_{c,S_i}} + 2T \sum_{\omega_n} \left[\frac{\Delta_{S_i}(x)}{\omega_n} - \sin \theta_{S_i}(i\omega_n, x) \right] = 0. \quad (4)$$

Here the function θ_{S_i} has been introduced as a unique Green's function defining the quasiparticle density of states N_{S_i} :

$$N_{S_i}(\epsilon, x)/N_{S_i}(0) = \text{Re} [\cos \theta_{S_i}(\epsilon, x)] \quad (5)$$

where $N_{S_i}(0)$ is the electronic density of states in the normal state at the Fermi surface.

In a multilayer structure the Usadel equations Eqs.3, 4 must be solved in each layer with the use of the appropriate boundary conditions. For convenience we substitute the coherence

length ξ_{S_i} by the quantity $\xi_{S_i}^* = \xi_{S_i} \sqrt{T_{c,S_i}/T_{c,S_1}}$, normalised to the critical temperature of the layer S_1 .

A Bilayer $S_1 - S_2$

Let us first consider the case of a bilayer. For any S_1 - S_2 system with $T_{c,S_2} < T_{c,S_1}$, the origin of the coordinates $x = 0$ is taken at the S_1 - S_2 interface. The region with $x > 0$ is S_1 and $x < 0$ corresponds to S_2 . The layers S_1 and S_2 have a thickness d_{S_1} and d_{S_2} , respectively. The boundary conditions can easily be written in terms of $\theta_{S_1(S_2)}$ [4]. At the S_1 - S_2 interface we have

$$\gamma_{BN} \xi_{S_2}^* \theta'_{S_2} = \sin(\theta_{S_1} - \theta_{S_2}) \quad (6)$$

$$\gamma \xi_{S_2}^* \theta'_{S_2} = \xi_{S_1} \theta'_{S_1}. \quad (7)$$

At the free interface of both S_1 and S_2 layers, the conditions are:

$$\theta'_{S_2}(-d_{S_2}) = 0 \quad ; \quad \theta'_{S_1}(d_{S_1}) = 0. \quad (8)$$

The parameters γ_{BN} and γ involved in the boundary conditions at the S_1 - S_2 interface are given by

$$\gamma_{BN} = \frac{R_B}{\rho_{S_2} \xi_{S_2}^*} \quad ; \quad \gamma = \frac{\rho_{S_1} \xi_{S_1}}{\rho_{S_2} \xi_{S_2}^*}. \quad (9)$$

These parameters can be understood as follows: γ is a measure of the strength of the proximity effect between the S_1 and S_2 metals, whereas γ_{BN} describes the effect of the boundary transparency between these layers. Here ρ_{S_1,S_2} are normal state resistivities and R_B is the product of the resistance of the S_1 - S_2 boundary and its area.

As is shown in Ref.[3], in the case of a thin S_2 layer where $d_{S_2}/\xi_{S_2}^* \ll 1$, the parameters defining the proximity effect are $\gamma_m = \alpha \gamma d_{S_2}/\xi_{S_2}^*$ and $\gamma_B = \alpha \gamma_{BN} d_{S_2}/\xi_{S_2}^*$. Here α is a correction factor which is a function of the ratio of critical temperatures $T_{c,S_2}/T_{c,S_1}$, and of the thickness of the layer S_2 . The dependence of the parameter α on $T_{c,S_2}/T_{c,S_1}$ can be found in Ref.[3].

B Trilayer $S_1 - S_2 - S_3$

We consider now the trilayer situation. This case is rather straightforward to solve with only few conditions. We first assume $d_{S_3} \ll \xi_{S_3}^*$. Again the origin of the coordinates $x = 0$ is taken at the S_1 - S_2 interface and the S_3 layer occupies the region $-d_{S_2} - d_{S_3} < x < -d_{S_2}$. As mentioned in [2], this approximation directly implies that pair potential and density of states in S_3 are constant through its whole thickness. The solution in the thin S_3 film is [2]

$$\tan \theta_{S_3} = \frac{\sin \theta_{S_2}(-d_{S_2}) + \gamma_{BN_2} \Delta_{S_3}}{\cos \theta_{S_2}(-d_{S_2}) + \gamma_{BN_2} \omega} \quad (10)$$

The boundary conditions at the interface S_1 - S_2 and at the free surface of S_1 can be derived from the general bilayer problem described above

$$\gamma_{BN_1} \xi_{S_2}^* \theta'_{S_2} = \sin(\theta_{S_1} - \theta_{S_2}) \quad (11)$$

$$\gamma_1 \xi_{S_2}^* \theta'_{S_2} = \xi_{S_1} \theta'_{S_1}. \quad (12)$$

$$\theta'_{S_1}(d_{S_1}) = 0. \quad (13)$$

An additional boundary condition can be introduced at the S_2 - S_3 interface, based on the fact that d_{S_3} is very small

$$\xi_{S_2}^* \theta'_{S_2}(-d_{S_2}) = \frac{\gamma_2 \omega \{ \sin \theta_{S_2}(-d_{S_2}) - \Delta_{S_3} \}}{\{ 1 + \gamma_{BN_2}^2 (\omega^2 + \Delta_{S_3}^2) + 2\gamma_{BN_2} \cos \theta_{S_2}(-d_{S_2}) [\omega + \Delta_{S_3} \sin \theta_{S_2}(-d_{S_2}) / \omega] \}} \quad (14)$$

Here the parameters γ_{BN_i} and γ_i are given by

$$\gamma_{BN_i} = \frac{R_{Bi}}{\rho_{S_{i+1}} \xi_{S_{i+1}}^*} ; \quad \gamma_i = \frac{\rho_{S_i} \xi_{S_i}^*}{\rho_{S_{i+1}} \xi_{S_{i+1}}^*}. \quad (15)$$

Again, the coherence lengths in S_2 and S_3 are normalized to T_{c,S_1} . Using a similar approach to those adopted previously, it is also straightforward to study the case of a very thin S_1 layer with arbitrary S_2 and S_3 film thicknesses.

III Applicability of the model to the clean limit

The main restriction of the model presented here is the use of dirty superconductors. It is straightforward to show that, in most cases, the clean limit does not need to be considered. The difference between clean and dirty limits lies in the presence of impurities or crystallographic dislocations in a dirty superconductor, acting as scattering centres for quasiparticles. If scattering centres are on average separated by a distance smaller than the coherence length, then the dirty limit applies. In other words, the dirty limit locally applies to a spherical region of radius equal to the coherence length, and centered at a scattering centre.

The physical presence of interfaces ensures the presence of scattering centres. As long as the interfaces affect several atomic layers of both superconductors, the boundary conditions are those of the dirty limit. Moreover, over a scale length equal to the coherence length in both films, any solutions for the pair potential and the densities of states are also governed by the same equations valid in a dirty superconductor. At depths larger than the coherence length, the fluctuations in pair potential and in densities of states are not significant, and the behaviour tends towards that of a bulk superconductor [2, 3]. Anderson's theorem [12] implies that in the case of a bulk superconductor, the solutions in the clean limit are the same as in the dirty limit. Hence, any solution for the pair potential and the density of states in regions of the films deeper than the coherence length, is expected to be a smooth interpolation between two dirty regions (in the case of a clean region separated by two rough boundaries), or a smooth extrapolation out of a single dirty region (in the case of a clean region located between a rough boundary and a flat one). The solutions related to such smooth interpolations or extrapolations are identical, independently of the use of the equations valid for the clean or for the dirty limit.

The clean limit only need to be considered in cases of atomically sharp interfaces, where the roughness σ_i of the S_1 - S_2 interface is of the order of or smaller than the interatomic distance of both S_1 and S_2 (typically around 4-5 Å). This case is extremely restrictive, and also technically difficult to achieve, even with the most advanced methods of epitaxial thin film depositions. It leads to the conclusion that the clean limit does not need to be considered.

IV Numerical results

In this section some typical examples of pair potential and density of states for the quasiparticles are determined and discussed for bi- and trilayers.

A Bilayer $S_1 - S_2$

For this bilayer, we have solved numerically the Usadel equations (3)-(4) by a selfconsistent procedure similar to that described in Ref. [3], but without the approximation $d_{S_2}/\xi_{S_2}^* \ll 1$. We start from the trial pair potentials $\Delta_{S_1(S_2)}(x)$ and find the solutions for $\theta_{S_1(S_2)}(\omega_n, x)$ in the Matsubara representation ($\epsilon = i\omega_n$). Using these solutions, the new pair potentials $\Delta_{S_1(S_2)}(x)$ are found from the selfconsistency equation. The iterations are repeated until convergence is achieved. Next, after the pair potentials are determined, we solve the equations (3)-(4) on the real energy axis ϵ . According to Equ.(5), this method provides spatially and energy resolved densities of states in both layers.

In order to demonstrate the validity of the approach and to be representative of the devices discussed in Section V, the cases of an Al-Nb and an Al-Ta bilayer ($T_{c,Al} = 1.18$ K, $T_{c,Ta} = 4.5$ K, $T_{c,Nb} = 9.25$ K) at $T = 0.3$ K are considered.

1 Al - Nb bilayer

The parameters for this simulation are $\gamma = 1.3$, $\gamma_{BN} = 2.7$, $d_{Al} = 1.7\xi_{Al}^*$ and $d_{Nb} = 4.35 \xi_{Nb}$. This choice of parameters is justified in Section V. The results are represented in Fig.1. The quantities represented here are the pair potential as a function of position in the bilayer (Fig. 1a) and the density of states at different positions (Fig. 1b). The density of states of Fig. 1b is shown at the free interface of S_1 (Nb) and of S_2 (Al) (solid lines), and on both sides of the Al-Nb interface (dashed lines). In Al, the density of states is peaking at an energy slightly higher than the gap, and then roughly decreases to 1 for infinite energies. Getting closer to the Nb film, a smaller peak is also visible around the energy gap of pure Nb. In Nb, the density of states is strongly peaking around Δ_{Nb} , and goes to 1 at infinite energy. Below Δ_{Nb} the density

of states is very much depressed as compared to the density of states in Al. However, it stays finite and importantly the energy gap is the same as in the Al film.

The position dependence of the energy gap is represented on Fig. 1a (dashed line in the middle). Clearly, it is not position dependent at all, despite the very strong fluctuations of the pair potential. It must be stressed that, even if Fig. 1b suggests a small density of states in Nb below Δ_{Nb} , this level actually corresponds to a significant number of states. As a matter of fact, the density of states at the free interface of Nb (solid line in Fig. 1b) at $0.3\Delta_{Nb}$ is $\simeq 1.43 \cdot 10^6 \text{states/meV}/\mu\text{m}^3$. Despite the fact that the gap is constant, the reduction in the DOS still has an effect on quasiparticle dynamics, since the quasiparticles in the energy range $0.3\Delta_{Nb} < \varepsilon < \Delta_{Nb}$ entering Nb are partially Andreev reflected. As shown in Ref. [13] the probability to enter the reduced density of states region is proportional to $N(\varepsilon)$.

2 Al – Ta bilayer

For this simulation the parameters are $\gamma = 0.05$, $\gamma_{BN} = 3.$, $d_{Al} = \xi_{Al}^*$ and $d_{Ta} = 1.18 \xi_{Ta}$. Again the choice of this set of parameters is explained in Section V. The results are represented in Fig 2. The value used for γ_{BN} is very similar to that used for the Nb-based sample, whereas the value used for γ is about 20 times lower. This has a direct impact on the shape of the pair potential (Fig. 2a) and the density of states (Fig. 2b). The discontinuity at the Ta/Al interface is extremely strong. The behaviour of Ta is almost bulk-like, with a constant pair potential and a steep peak of the density of states at around Δ_0^{Ta} . However there is still a considerable amount of states available in Ta below Δ_0^{Ta} (typically $0.1 \times 2N_0 = 8.1 \cdot 10^6 \text{ states/meV}/\mu\text{m}^3$). The fluctuations of the pair potential and the density of states within Al are also rather small, though a clear contribution from Ta remains visible at Δ_0^{Ta} . Despite the very weak coupling between Al and Ta, the gap is still constant through the whole device thickness. Such a strong discontinuity at the interface emphasizes the role of quasiparticle confinement in Al, due to Andreev reflections.

B Trilayer $S_1 - S_2 - S_3$

Next we consider two representative examples of a trilayer system: Al-Nb-NbN and Al-Nb-Ta, which also do have practical applications. The inclusion of a thin NbN passivation layer on the top electrode of an Al-Nb STJ in place of the natural niobium oxides reduces the quasiparticle loss rate, thereby enhancing the probability of multiple tunnel processes [14]. On the other hand the deposition of a thin Nb layer on top of the Al facilitates the deposition of the top Ta in Al-Ta STJs. The best Ta based devices, in terms of detection of optical photons, have a top electrode of this kind.

In both cases the Al layer has a thickness $d_{Al} = 0.1\xi_{Al}^*$, for which the thin layer approximation works reasonably well, while no limitation on the thickness of other layers was introduced. The method of numerical solution in this case is similar to that for a bilayer with additional boundary conditions (14), as described in the previous section.

1 Al - Nb - NbN trilayer

In the case of Al-Nb-NbN we have taken thicknesses $d_{Nb}/\xi_{Nb}^* = 3$. and $d_{NbN}/\xi_{NbN} = 3$, and $T_{c,NbN} = 14K$. The parameters of the Al-Nb interface are $\gamma_2 = 1.3$ and $\gamma_{BN_2} = 2.7$, as in the previous example. For the Nb-NbN interface $\gamma_1 = 2$ is expected from the resistivity ratio, while for the barrier transparency parameter we have assumed $\gamma_{BN_1} = 1$. The results of calculations of the spatial distribution of the pair potential in the Al-Nb-NbN trilayer are shown in Fig.3a. The dashed line shows the energy gap, which is again constant across the trilayer. The densities of states are shown in Fig.3b at the free interface of NbN, $x = 3\xi_{NbN}$, (solid line), on both sides of the NbN-Nb interface, $x = \pm 0$, (dashed lines), on the Nb side of the Nb-Al interface, $x = -3\xi_{Nb}$ (solid line) and in Al (dotted line). Again, in Al the density of states is peaking at an energy slightly higher than the gap. The magnitude of the gap is higher than in the case of Fig.1 due to the smaller thickness of Al and the influence of the NbN layer. Note, the gap in Al is now as big as about half of the gap of pure NbN, Δ_{NbN} . The density of states at the free interface of NbN, $x = 3\xi_{NbN}$, peaks around Δ_{NbN} , while a lot of states are also present in this

layer at $\varepsilon < \Delta_{NbN}$.

2 Al – Nb – Ta trilayer

In the case of Al-Nb-Ta we have taken thicknesses $d_{Nb}/\xi_{Nb}^* = 0.5$ and $d_{Ta}/\xi_{Ta} = 3$, and $T_{c,Ta} = 4.47K$. The parameters of the Nb-Ta interface are assumed to be $\gamma_1 = 0.3$ and $\gamma_{BN_1} = 3.8$. For the Al-Nb interface $\gamma_2 = 1.3$ and $\gamma_{BN_2} = 2.7$ were chosen again. The distribution of the pair potential, the energy gap and the local densities of states are shown in Fig.4a,b. The notations in Fig.4b are the same as in Fig.3b with NbN and Ta interchanged. As is seen from comparison of Figs.3 and 4, the energy gap in the Al-Nb-Ta trilayer is lower than that in the Al-Nb-NbN. This is expected, since the only difference between these two cases is that the high gap material, NbN, is substituted by the low gap one, Ta. Moreover, the peaks of the density of states in Nb are sharper in the case of Al-Nb-Ta trilayer. The reason is the more homogeneous distribution of the pair potential in this case, as is seen from Fig.4a.

V Application

The STJ would represent a typical but not exclusive example of an application of multi-layered superconducting thin films. Such devices used as photon detectors have produced good results in terms of energy resolution, charge output and quantum efficiency, for photon energies from the near infrared to X-rays [15]-[20]. The most important results currently achieved can be summarised as follows: Ta/Al junctions provide a typical response of up to 10^5 electrons per eV of the detected photon, at a temperature of 300 to 400 mK; the associated measured energy resolution is within a few percents of the predicted theoretical limit; the quantum efficiency at UV wavelengths is about 60%; the longest wavelength detected is currently $2\mu\text{m}$, with the possibility to extend this limit to $10\mu\text{m}$; the same junctions operate also at x-ray energies as high as 6 keV, with a quantum efficiency of about 10% and an energy resolution of about 40 eV FWHM. Very encouraging results have been also achieved with Nb/Al [20] and NbN/Nb [14] STJ's. At x-ray energies (6 keV), the best results currently achieved yield an energy resolution

of 12 eV for 5.9 keV photons, with an Al-based junction working at 50 mK [21].

A major problem to be addressed is the ability to predict the junctions response to photon absorption. This response can be modified by changing such variables as film thickness, film quality, and overall device dimensions. Especially, the performance of existing devices is still difficult to predict when the proximity effect plays a significant role. In particular, a significant difference in junction behaviour has been observed when irradiated by x-rays, as opposed to optical photons ([20]). Note while the trend in X-ray responsivity reflects the generally increasing role of quasiparticle self-recombination with increasing photon energies, the details of this response have been difficult to model using existing theories. Also, addressing adequately the problems of energy non-linearity ([22]-[24]) and quasiparticle trapping ([25]) requires a detailed knowledge of the proximity effect theory.

A Applicability of previous models

The aim of this section is to show that the existing models for the proximity effect are for very specific cases and regimes only and need generalisation in order to explain the performance of an STJ.

The type of junctions in which the energy dependence of the responsivity is difficult to account for are described in [26]. They essentially consist of symmetrical Nb/Al/AlO_x/Al/Nb junctions deposited on super-polished *R*-plane sapphire, with 100 nm of Nb and 15 to 120 nm of Al. The base electrode is epitaxial, whilst the top is polycrystalline. The polycrystalline film is usually covered by a thin NbO layer, followed by a Nb₂O₅ layer (~ 5 nm in total), due to the normal exposure to air. Note, the bandgap is much smaller in Al than in Nb. The Al layer represents the S_2 layer, and the Nb the S_1 layer.

A typical value for the coherence length in bulk, clean Al at 0 K is $\xi_{Al}(0) \sim 1.6 \mu\text{m}$. For the polycrystalline film (superscripts p indicates polycrystalline), the electron mean free path l_{Al}^p is limited by the grain size. Using a Transmission Electron Microscope (TEM), the grain size in the polycrystalline Al film has been estimated at about 40 nm. In the dirty limit, the coherence

length is given by $\xi_{Al}^p = \sqrt{l_{Al}^p \xi_{Al}(0)/3} \simeq 147$ nm, and $\xi_{Al}^{*,p} = \xi_{Al}^p \sqrt{T_{c,Al}/T_{c,Nb}} \simeq 53$ nm. Thus the condition of the dirty limit for the polycrystalline films S_1 and S_2 is not actually valid. Furthermore, this coherence length is precisely in the middle of the range of Al thicknesses available, and the condition of small Al thickness is also not satisfied. As for the epitaxial film (superscripts e), the mean free path l_{Al}^e is not limited by the grain size anymore, but it is simply constrained by the boundary scattering due to the thickness of the electrode (220 nm) and thus is always far lower than $\xi_{Al}(0)$. This conclusion is consistent with RRR (resistance residual ratio) measurements, which lead to an average mean free path of ~ 150 nm over the whole electrode. The coherence length $\xi_{Al}^{*,e}$ can therefore be assumed to be governed by a dirty environment, and will not exceed $\xi_{Al}^{*,p} \sqrt{l_{Al}^e/l_{Al}^p} < 120$ nm. This is not very large compared to either l_{Al}^e or d_{Al} . As a consequence, in the epitaxial film, none of the assumptions associated with the dirty limit and with a thin Al layer are valid.

In Nb, $\xi_{Nb}(0) \sim 38$ nm. This is very close to the grain size in the polycrystalline film, implying that the Nb polycrystalline film is in between the dirty and the clean limit. If the layer S_1 was assumed to be dirty, the coherence length is $\xi_{Nb}^p \sim 23$ nm. In reality, it is somewhere between 23 and 38 nm. In any case, the dirty limit does not apply. In the epitaxial layer, RRR measurements have determined an electron mean free path $l_{Nb}^e \simeq 150$ nm; here we are clearly in the clean limit, constrained by boundary scattering, such that for a Nb film of thickness 100 nm (applicable for all examples described herein), the condition of a thick S_1 layer is not fulfilled.

B Application of the generalised proximity effect model

The model has been applied to two different STJ layups. The first one is a symmetrical Nb based STJ with 100nm of Nb and 90 nm of Al. The second is a symmetrical Ta based STJ with 100nm of Ta and 55 nm of Al. In order to determine the density of states and the order parameters, all the input parameters for the proximity effect model have to be established. These parameters are the critical temperature, the ratio between the thickness of each layer and the coherence

length, and the interface parameters.

The coherence length in a non bulk configuration can be expressed in terms of the bulk coherence length ξ_0 and of the electron mean free path l . If the superconductor is in the clean limit, this relation is

$$\frac{1}{\xi} = \frac{1}{\xi_0} + \frac{1}{l}. \quad (16)$$

In the dirty limit, where $l \ll \xi$, one has

$$\xi = \sqrt{\frac{\hbar D}{2\pi k T_c}}. \quad (17)$$

Assuming the clean limit in epitaxial base films and the dirty limit in polycrystalline top films, limiting the mean free path to the grain size (40 nm) in polycrystalline films, the values of $\xi_{Nb} \sim 23$ nm, $\xi_{Al} \sim 147$ nm and $\xi_{Ta} \sim 85$ nm were found. These values are actually averages between the values found for polycrystalline and epitaxial films. Using these values we determine the ratios of thickness to normalised coherence length as used for the numerical simulations in Sections IV A 1 and 2.

The method chosen to determine the values of the interface parameters is to compare an experimentally determined value with the theoretical estimate, as derived from a simple analytical expression for this value, which includes the densities of states. The quantities to be fitted to the model were chosen to be the energy gap as a function of temperature and the critical current as a function of temperature. Both quantities are easily found experimentally from the junctions I-V curve characteristics. The critical current I_c through the junction is calculated in the following way[3]

$$\frac{e I_c R_N}{2\pi T_c} = \frac{T}{T_c} \sum_{\omega_n > 0} \sin \theta_1(\omega_n) \sin \theta_2(\omega_n), \quad (18)$$

where R_n is the normal-state resistance of the junction, and $\theta_{1(2)}(\omega_n)$ is the local Green's function in the vicinity of the barrier in electrode 1 and 2 respectively. Both electrodes are assumed to be identical, therefore simplifying Eq. (18), since $F_1 = F_2$, and thereby ensuring a unique set of (γ, γ_{BN}) parameters for the whole junction.

Figs. 5a and 6a show the model values compared to the experimental data of the energy gap as a function of device temperature for the Nb and the Ta based STJs respectively. Figs 5b and 6b show essentially the same information, but this time in regard to the critical current.

The fits to the experimental points correspond to model values with $\gamma = 1.3$, $\gamma_{BN} = 2.7$ for the Nb based STJ and $\gamma = 0.05$, $\gamma_{BN} = 3$ for the Ta based STJ. In both cases the fit of the bandgap is satisfactory, while the critical current of the Nb based device is slightly too low.

Using these model derived values of the parameters we obtain the results presented in sections IV A 1 and 2.

C Dependence of the interface parameters on film thickness

We will now analyse how the interface parameters vary when the thicknesses of the films change, all other parameters staying the same. Assuming that the dirty limit is valid, we can replace the coherence length by its expression in the dirty limit:

$$\xi = \sqrt{\frac{\xi_0 l}{3}} \quad (19)$$

This gives the following expressions for the interface parameters:

$$\gamma_{BN} = C_{\gamma_{BN}} \sqrt{\frac{T_{c,1} l_2}{T_{c,2}}} ; \quad \gamma = C_{\gamma} \sqrt{\frac{T_{c,1} l_2}{T_{c,2} l_1}} \quad (20)$$

where the constants C_{γ} and $C_{\gamma_{BN}}$ are defined by:

$$C_{\gamma_{BN}} = \frac{R_B}{\rho_2 l_2} \sqrt{\frac{3}{\xi_{0,2}}} ; \quad C_{\gamma} = \frac{\rho_1 l_1}{\rho_2 l_2} \sqrt{\frac{\xi_{0,1}}{\xi_{0,2}}} \quad (21)$$

These two constants are independent of the film thickness. C_{γ} depends only on the nature of the two films involved, whereas $C_{\gamma_{BN}}$ depends also on the macroscopic properties of the interface. The only variables depending on the film thickness are the critical temperature and the mean free path.

The critical temperature as a function of film thickness can be determined according to the model of Cooper [28]. This model states that superconductivity is lost in a thin surface layer b_t

due to a reduction in the electron density of states near the surface. The critical temperature dependence according to this model is:

$$T_c = T_{c,0} \left(1 - \frac{2b_t}{N\nu t} \right), \quad (22)$$

where $T_{c,0}$ is the critical temperature of the bulk material, N is the electron density of states at the Fermi level, ν the bulk interaction potential and t the film thickness.

The bulk mean free path at low temperature l_0 (just above the critical temperature) can be found via the bulk mean free path at 300K, $l_{0,300}$, and the residual resistance ratio (RRR_b) of a thick film:

$$l_0 = RRR_b l_{0,300}. \quad (23)$$

We can then calculate the mean free path in a thin film ($t \ll l_0$), using [29]:

$$l = \frac{3t}{4} \left(\ln \frac{l_0}{t} + 0.423 \right). \quad (24)$$

Using the interface parameters found for a Nb based STJ with 45 nm of Al and the basic material constants for Nb and Al (table 1) appearing in equations (19)-(24), we can determine the interface constants C_γ and $C_{\gamma_{BN}}$. Except for the factor $N\nu$ (cfr. eq. 22), which was determined in Ref. [30], all values in table 1 were derived from experiments on Nb thin films or Nb/Al/AlOx/Al/Nb multilayers. For these films the critical temperature and RRR were measured as a function of film thicknesses. A fit to these experimental points provided the values of b_t and $T_{c,0}$.

Using equations (22) and (24) we then calculate the values of the interface parameters for different Al film thicknesses. The theoretical and experimental values of the interface parameters for symmetrical Nb/Al STJs with Al film thicknesses of 15, 30, 45 and 90 nm and a constant Nb film thickness of 100nm can be found in table 2. The experimental values were determined in exactly the same way as described in the previous section. The correspondence between experiment and theory is very good, when we take into account the rather large

uncertainties we are dealing with respect to the numerous parameters involved. Note that including the γ_{BN} parameter in the discussion is important, as it is not small and has a strong effect on the density of states in the two films. This is in accordance with the results obtained by Zehnder et al. ([31]). Nevertheless the dependence on film thickness is rather complex for both interface parameters. No clear square root dependence for γ or linear dependence for γ_{BN} was observed, as stated in ref [31].

VI CONCLUSIONS

A model describing the proximity effect for any kind of superconducting bilayer, in terms of thickness, critical temperature and cleanliness, and superconducting trilayers with a thin third layer has been presented. It has been proposed that any existing samples, even if very clean, would obey to these equations which are valid in the dirty limit, because of the presence of imperfections at the boundary. Only in very specific cases of extremely thin and smoothly deposited layers (with an rms roughness at the interface of the order of the interatomic distance in both materials) would the model not apply. This model has been presented and examined experimentally for typical values of the parameters involved for tunnel junctions, using thicknesses intermediate between the extreme cases discussed in previous publications. Finally, the model has been shown to be very effective in determining the various important parameters for practical cases, using the current-voltage characteristics of STJ's (energy gap and critical current as a function of temperature).

VII Tables

	RRR_b	$l_{0,300}$	b_t	$N\nu$	$T_{c,0}$	ξ_0
	/	nm	nm	/	K	nm
Nb	25	2.2	0.26	0.35	9.2	40
Al	4	10.3	0.2	0.175	1.2	1600

Table 1: Basic parameters for Nb and Al

	γ (th.)	γ (exp.)	γ_{BN} (th.)	γ_{BN} (exp.)
15nm Al	1.07	0.9	1.85	1.5
30nm Al	1.32	1.2	2.3	2.2
45nm Al	1.6	1.6	2.7	2.7
90nm Al	1.6	1.3	2.7	2.7

Table 2: Comparison of theoretical and experimental values of the interface parameters for Nb/Al STJs with different Al film thicknesses.

References

- [1] W.L. McMillan, Phys.Rev. **175**, 537 (1968).
- [2] A.A. Golubov, E.P. Houwman, J.G. Gijsbertsen, J. Flokstra, and H. Rogalla, Phys.Rev.B **49**, 12953 (1994).
- [3] A.A. Golubov, E.P. Houwman, J.G. Gijsbertsen, V.M. Krasnov, M.Yu. Kupriyanov, J. Flokstra, and H. Rogalla, Phys.Rev.B **51**, 1073 (1995).
- [4] M.Yu. Kupriyanov and V.F. Lukichev, Zh.Eksp.Teor.Fiz. **94**, 139 (1988) [Sov.Phys.JETP **67**, 1163 (1988)].
- [5] A.A. Golubov and M.Yu. Kupriyanov, Zh.Eksp.Teor.Fiz. **96**, 120 (1989).
- [6] W. Belzig, C. Bruder and G. Schon, Phys.Rev.B **54**, 9443 (1996).
- [7] A.A. Abrikosov, L.P. Gor'kov, I.E. Dzyaloshinskii, Methods of Quantum Field Theory in Statistical Physics, (1962).
- [8] G. Eilenberger, Z.Phys. **214**, 195 (1968).
- [9] K.D. Usadel, Phys. Rev. Lett. **25**, 507 (1970).
- [10] G.M. Eliashberg, Zh.Eksp.Teor.Fiz. **61**, 1254 (1971) [Sov.Phys.JETP **34**, 668 (1972)].
- [11] A.I. Larkin and Yu.N. Ovchinnikov, Zh.Eksp.Teor.Fiz. **73**, 299 (1977) [Sov.Phys.JETP **41**, 960 (1977)].
- [12] P.G. de Gennes. Superconductivity of Metals and Alloys (New York, Benjamin, 1966), p.157.
- [13] B. A. Aminov, A.A. Golubov and M.Yu. Kupriyanov, Phys.Rev.B **53**, 365 (1996).
- [14] N. Rando, P.Verhoeve, A.Poelaert, A.Peacock, D.J. Goldie, J. Appl. Phys. **83**, 10 (1998).

- [15] N. Rando, A. Peacock, A. van Dordrecht, C. Foden, R. Engelhardt, B.G. Taylor, P. Garé, J.M. Lumley, and C. Pereira, *Nucl.Instr.Met.Ph.Res.A* **313**, 173 (1992).
- [16] P. Verhoeve, N. Rando, J. Verveer, A. Peacock, A. van Dordrecht, P. Videler, M. Bavdaz, D.J. Goldie, T. Lederer, F. Scholze, G. Ulm, and R. Venn, *Phys.Rev.B* **53**, 809 (1996).
- [17] C.A. Mears, S.E. Labov, and A.T. Barfknecht, *Low Temp.Phys.* **92**, 561 (1993).
- [18] A. Peacock, P. Verhoeve, N. Rando, A. van Dordrecht, B.G. Taylor, C. Erd, M.A.C. Perryman, R. Venn, J. Howlett, D.J. Goldie, J. Lumley, and M. Wallis, *Nature* **381**, 135 (1996).
- [19] A. Peacock, P. Verhoeve, N. Rando, C. Erd, M. Bavdaz, B.G. Taylor, and D. Perez, *Astron. Astrophys. Suppl. Ser.* **127**, 497 (1998).
- [20] P. Verhoeve, N. Rando, A. Peacock, A. van Dordrecht, A. Poelaert, D.J. Goldie, R. Venn, *J.Appl.Phys.* **83**, 11, 6118 (1998).
- [21] P. Hettl et al., *Proceedings of EDXRS-98, Bologna, Italy, June 7-12*, 1(1998).
- [22] D. J. Goldie, P. L. Brink, C. Patel, N. E. Booth, and G. L. Salmon, *Appl. Phys. Lett.* **64**, 3169 (1994).
- [23] P. de Korte, M.L. van den Berg, M.P. Bruijn, M. Frericks, J.B. le Grand, J.G. Gijsbertsen, E.P. Houwman, and J. Flokstra, *Proc. SPIE* **1743**, 24 (1992).
- [24] S.B. Kaplan, C.C. Chi, D. Langenberg, J.J. Chang, S. Jafarey, and D. Scalapino, *Phys. Rev. B* **14**, 4854 (1976).
- [25] N. Booth, *Appl. Phys. Lett.* **50**, 293 (1987).
- [26] A. Poelaert, P. Verhoeve, N. Rando, and A. Peacock, *Proc. SPIE* **2808**, 523 (1996).
- [27] K.E. Gray, *J.Phys.F: Metal Phys.* **1**, 290 (1971).

- [28] L.N. Cooper, Phys. Rev. Lett. **6**, 689 (1961).
- [29] D. Movshovitz, N. Wiser, Phys. Rev. B **41**, 10503 (1990).
- [30] R. Meservey, B. B. Schwartz, , *Superconductivity* (Vol.1, R.D. Parks (ed.), Dekker, New York, 1969), p.12
- [31] A. Zehnder, Ph. Lerch, S.P. Zhao, Th. Nussbaumer, E.C. Kirk, H.R. Ott, Phys. Rev. B, **59** (1999) 8875.

Captions for figures

Figure 1:

Typical output for Al-Nb. Pair potential (a) and density of states (b) for $\gamma = 1.3$ and $\gamma_{BN} = 2.7$, with $d_{S_2} = 1.7 \xi_2^*$ and $d_{S_1} = 4.35 \xi_1$. (a) The upper dashed line is the bulk energy gap of Nb. The lower dashed line is the bulk energy gap of Al. The intermediate dashed line is the resulting energy gap, as determined from Fig 1 (b). (b) The densities of states are represented for both materials at the free interface (solid lines) and at the S_1 - S_2 interface (dashed lines).

Figure 2:

Typical output for Al-Ta. Pair potential (a) and density of states (b) for $\gamma = 0.05$ and $\gamma_{BN} = 3.$, with $d_{S_2} = \xi_2^*$ and $d_{S_1} = 1.18 \xi_1$. (a) The upper dashed line is the bulk energy gap of Ta. The lower dashed line is the bulk energy gap of Al. The intermediate dashed line is the resulting energy gap, as determined from Fig 2 (b). (b) The densities of states are represented for both materials at the free interface (solid lines) and at the S_1 - S_2 interface (dashed lines).

Figure 3:

Typical output for Al-Nb-NbN. Pair potential (a) and density of states (b) for $\gamma_1 = 2.$, $\gamma_{BN_1} = 1.$, $\gamma_2 = 1.3$ and $\gamma_{BN_2} = 2.7$ with $d_{S_3} = 0.1 \xi_3^*$, $d_{S_2} = 3 \xi_2^*$ and $d_{S_1} = 3 \xi_1$. (a) The upper dashed line is the bulk energy gap of NbN. The lower dashed line is the bulk energy gap of Al. The intermediate dashed line is the resulting energy gap, as determined from Fig 3 (b). (b) The densities of states are represented for NbN at the free interface (solid line), at the S_1 - S_2 interface (dashed lines) and at the $S_2 - S_3$ interface (dotted lines).

Figure 4:

Typical output for Al-Nb-Ta. Pair potential (a) and density of states (b) for $\gamma_1 = 0.3$, $\gamma_{BN_1} = 3.8$, $\gamma_2 = 1.3$ and $\gamma_{BN_2} = 2.7$ with $d_{S_3} = 0.1 \xi_3^*$, $d_{S_2} = 0.5 \xi_2^*$ and $d_{S_1} = 3 \xi_1$. (a) The upper dashed line is the bulk energy gap of Nb. The lower dashed line is the bulk energy gap of Al. The intermediate dashed line is the resulting energy gap, as determined from Fig 4 (b). (b) The densities of states are represented for Ta at the free interface (solid line), at the S_1 - S_2

interface (dashed lines) and at the $S_2 - S_3$ interface (dotted lines).

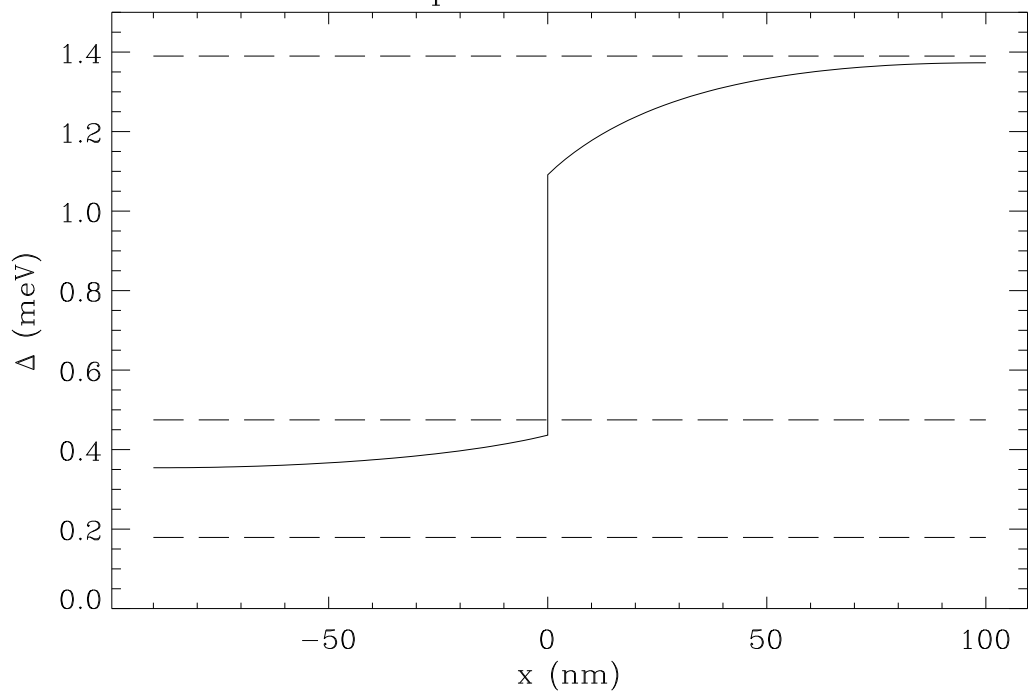
Figure 5:

Energy gap (a) and critical current (b) as a function of temperature for the Al-Nb STJ ($d_{Al} = 90nm$, $d_{Nb} = 100nm$). The data (diamonds) is fitted using $\gamma = 1.3$ and $\gamma_{BN} = 2.7$. The expected experimental uncertainty for the data points is also represented.

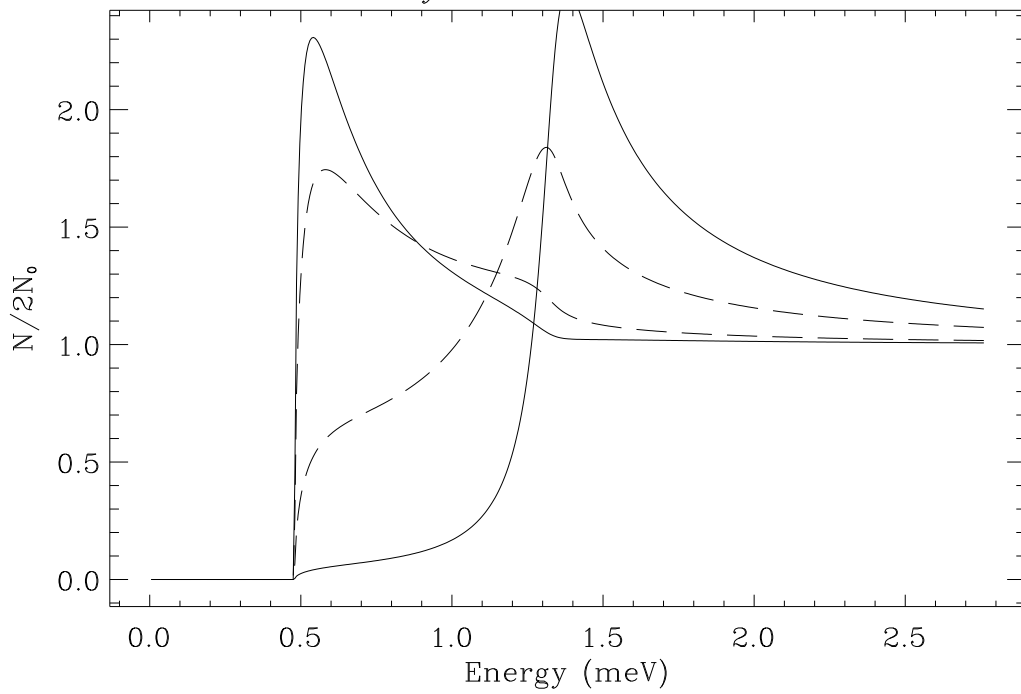
Figure 6:

Energy gap (a) and critical current (b) as a function of temperature for the Al-Ta STJ ($d_{Al} = 55nm$, $d_{Ta} = 100nm$). The data (diamonds) is fitted using $\gamma = 0.05$ and $\gamma_{BN} = 3$.

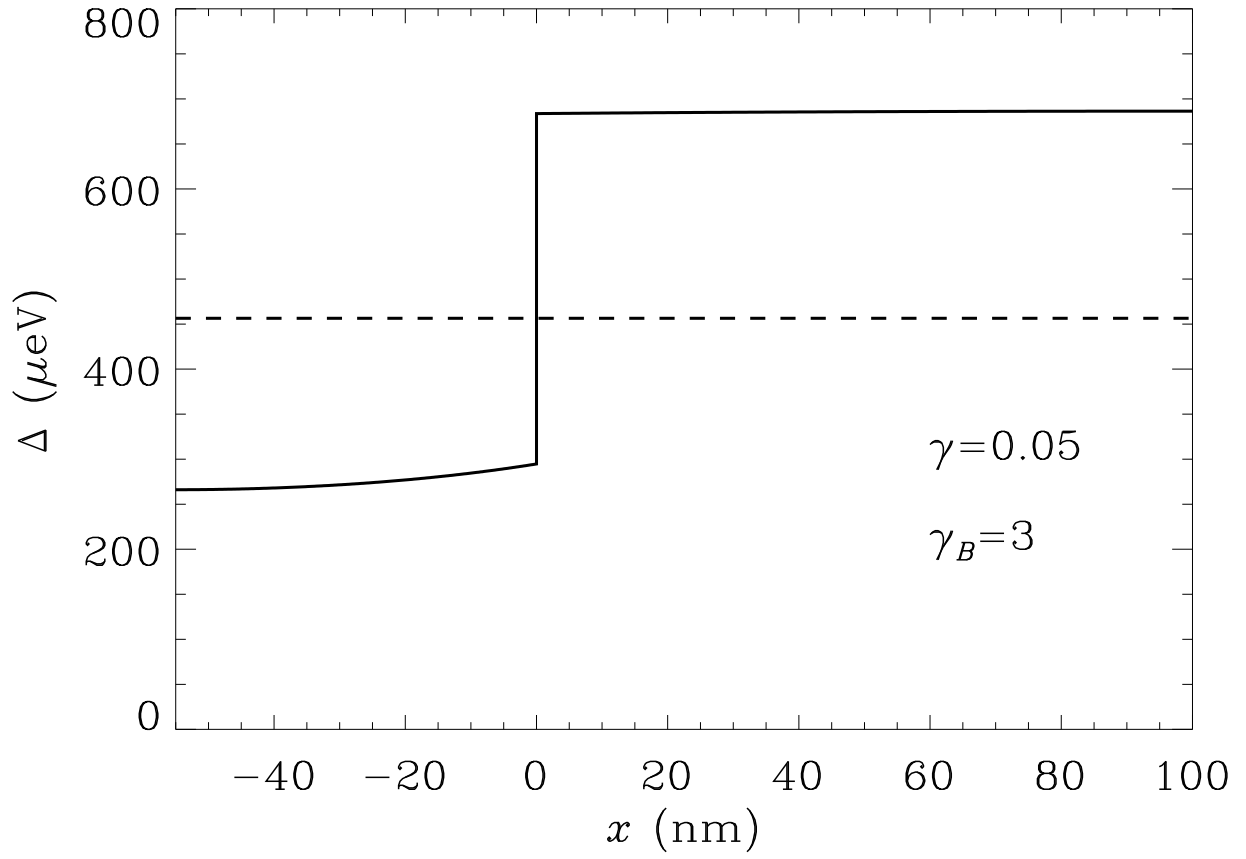
Pair potential for Al-Nb



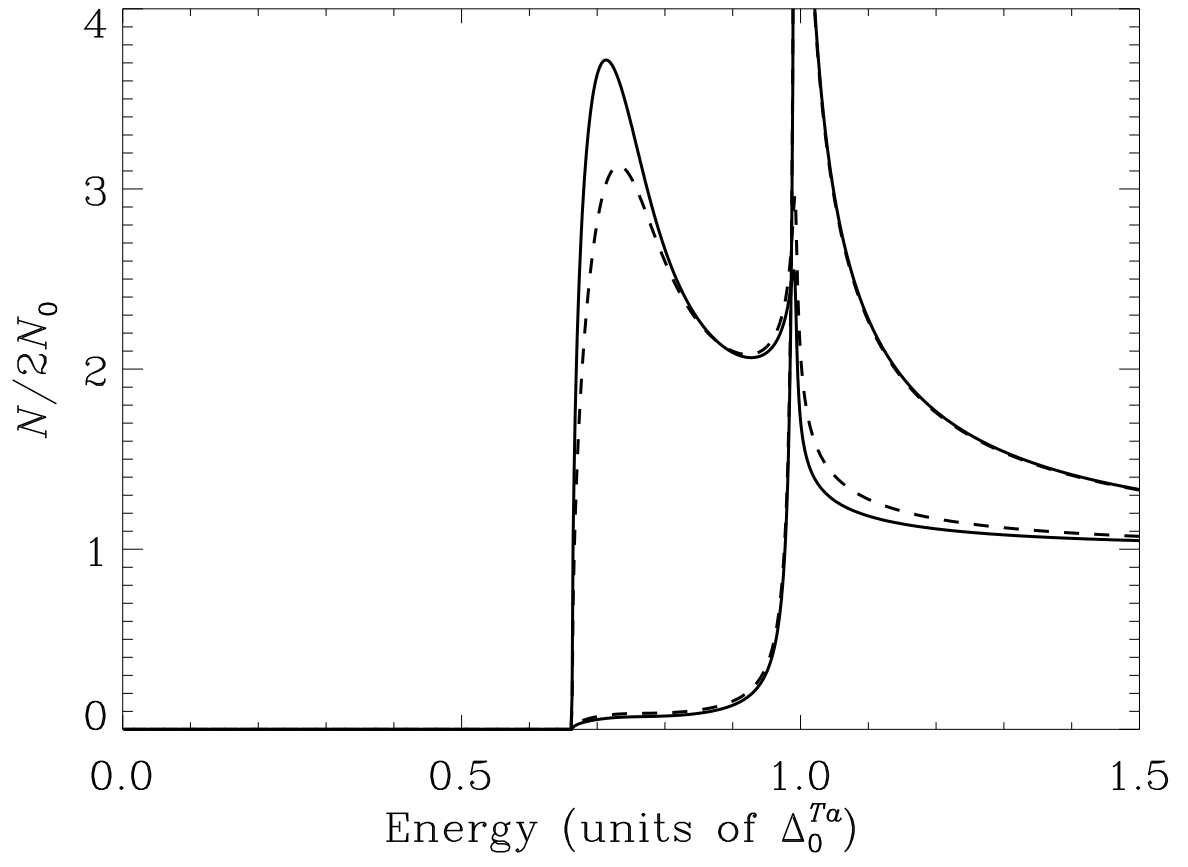
density of states for Al-Nb



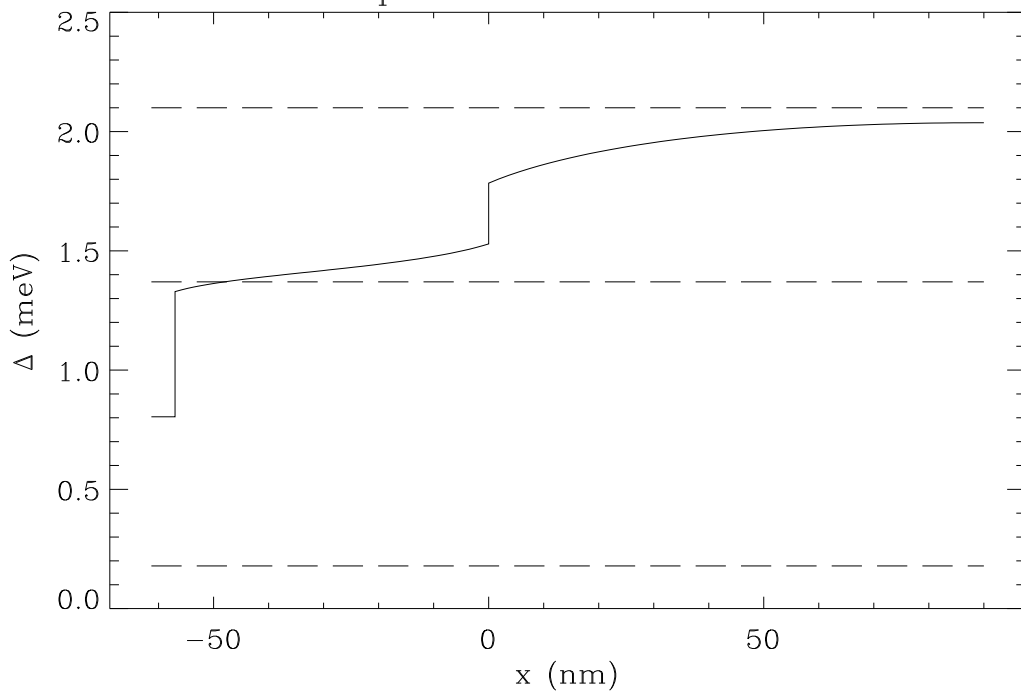
Pair potential for Ta01



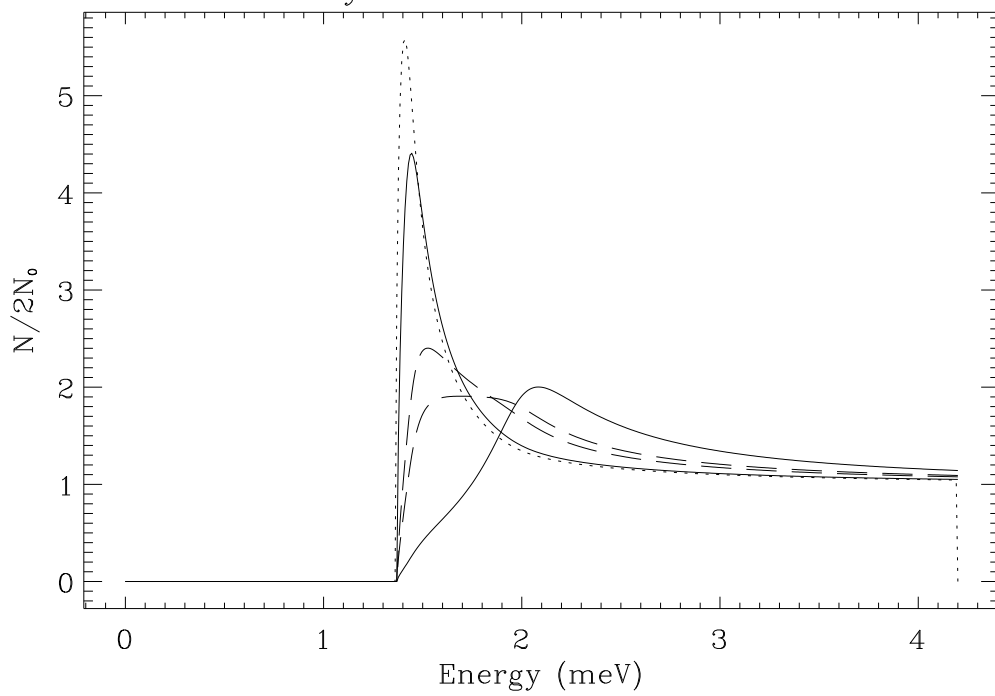
Density of states for Ta01



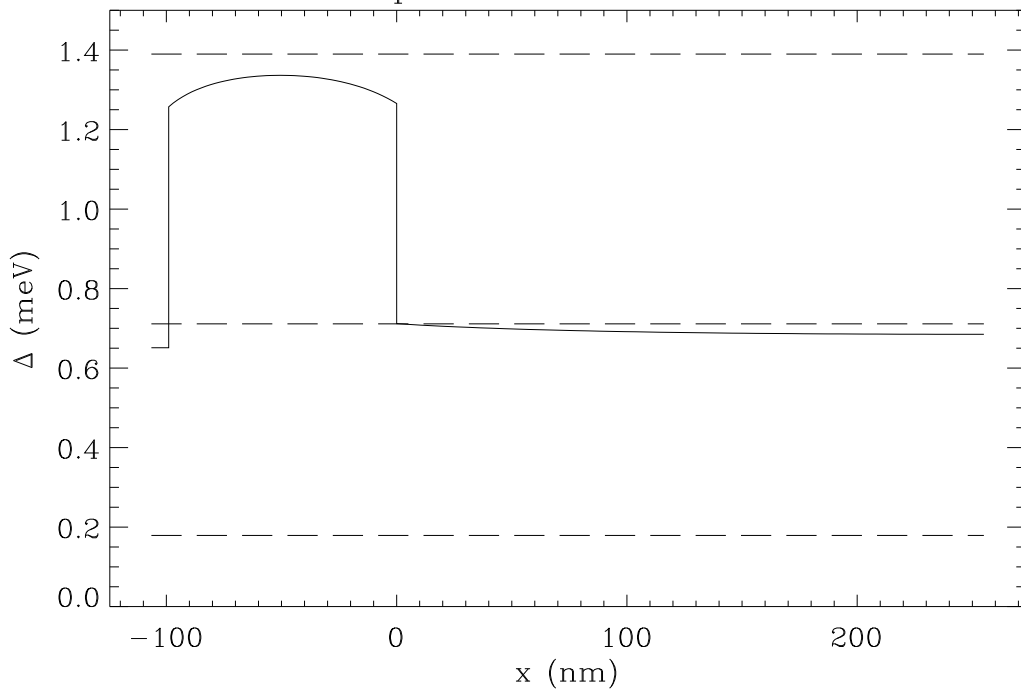
Pair potential for Al-Nb-NbN



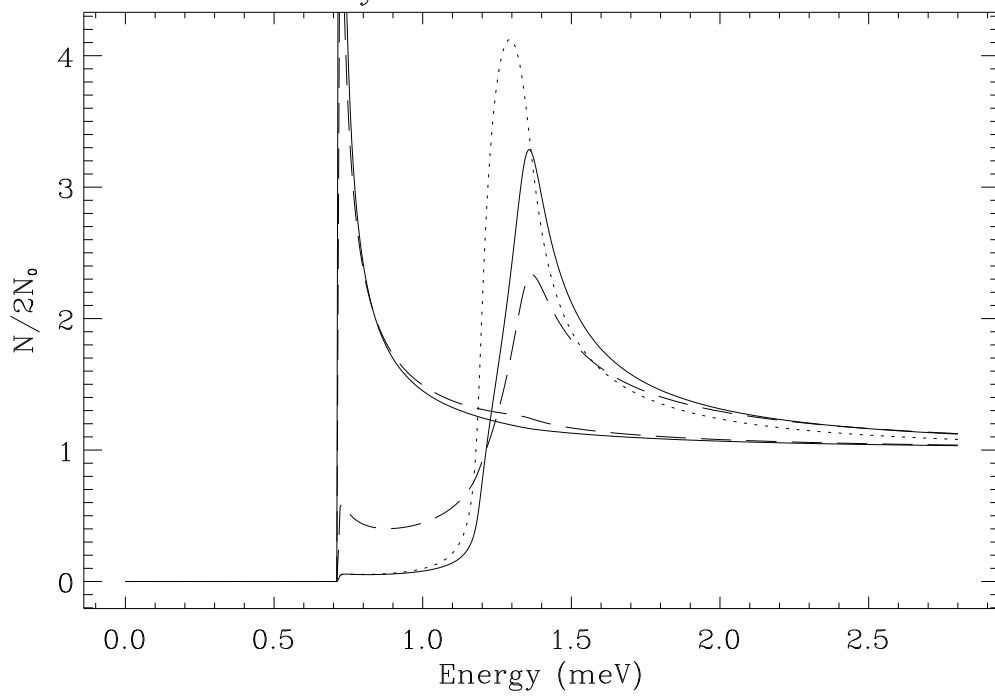
density of states for Al-Nb-NbN

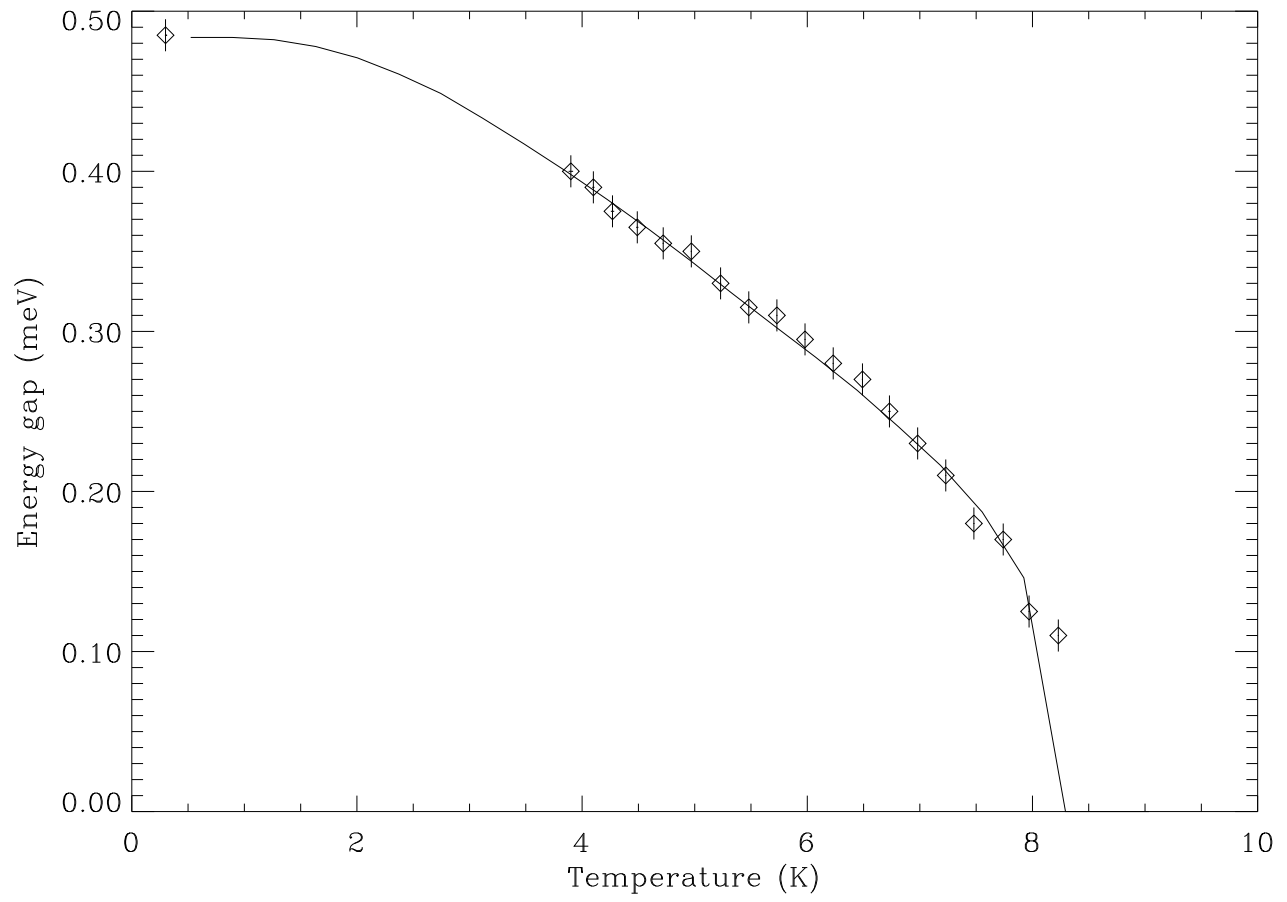


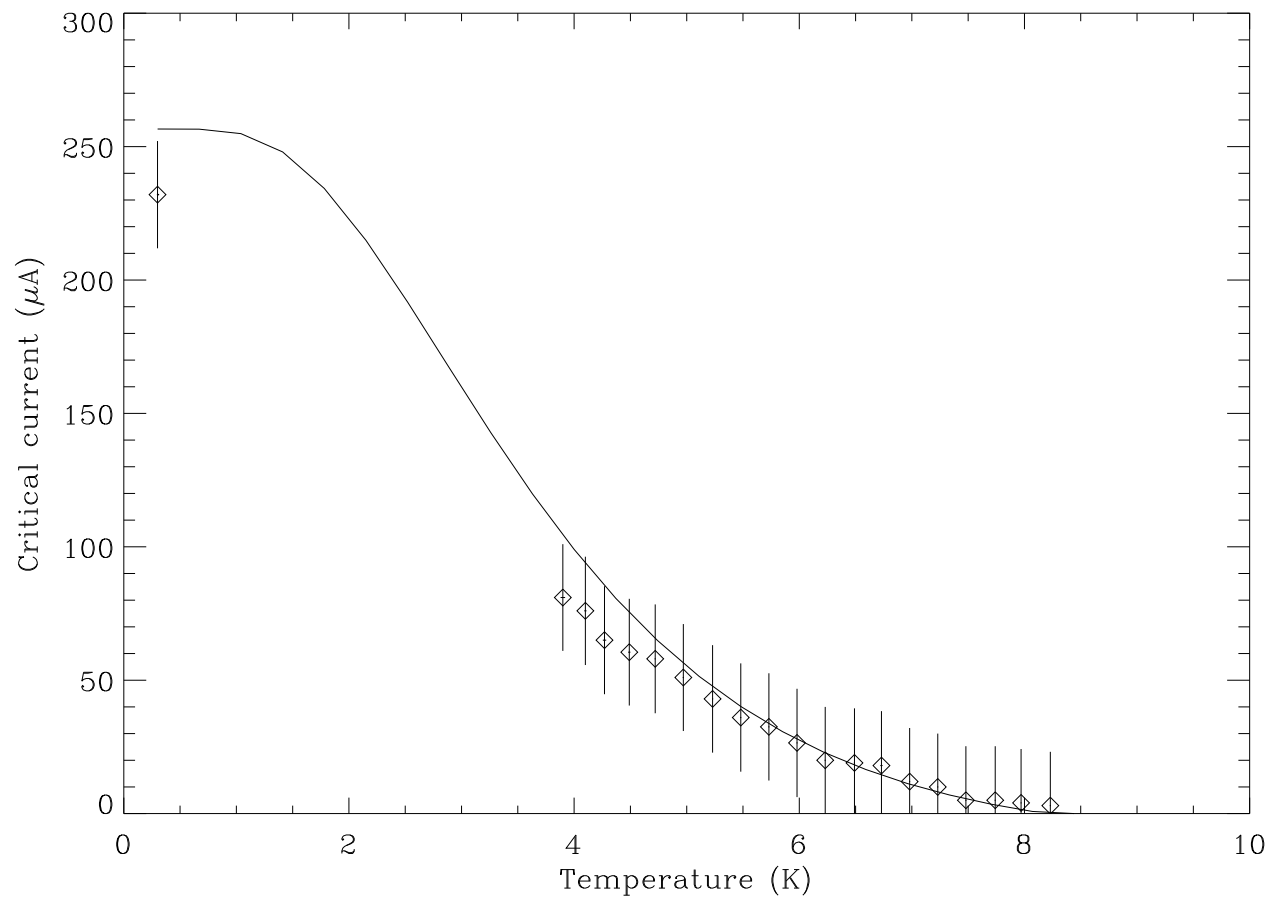
Pair potential for Al-Nb-Ta



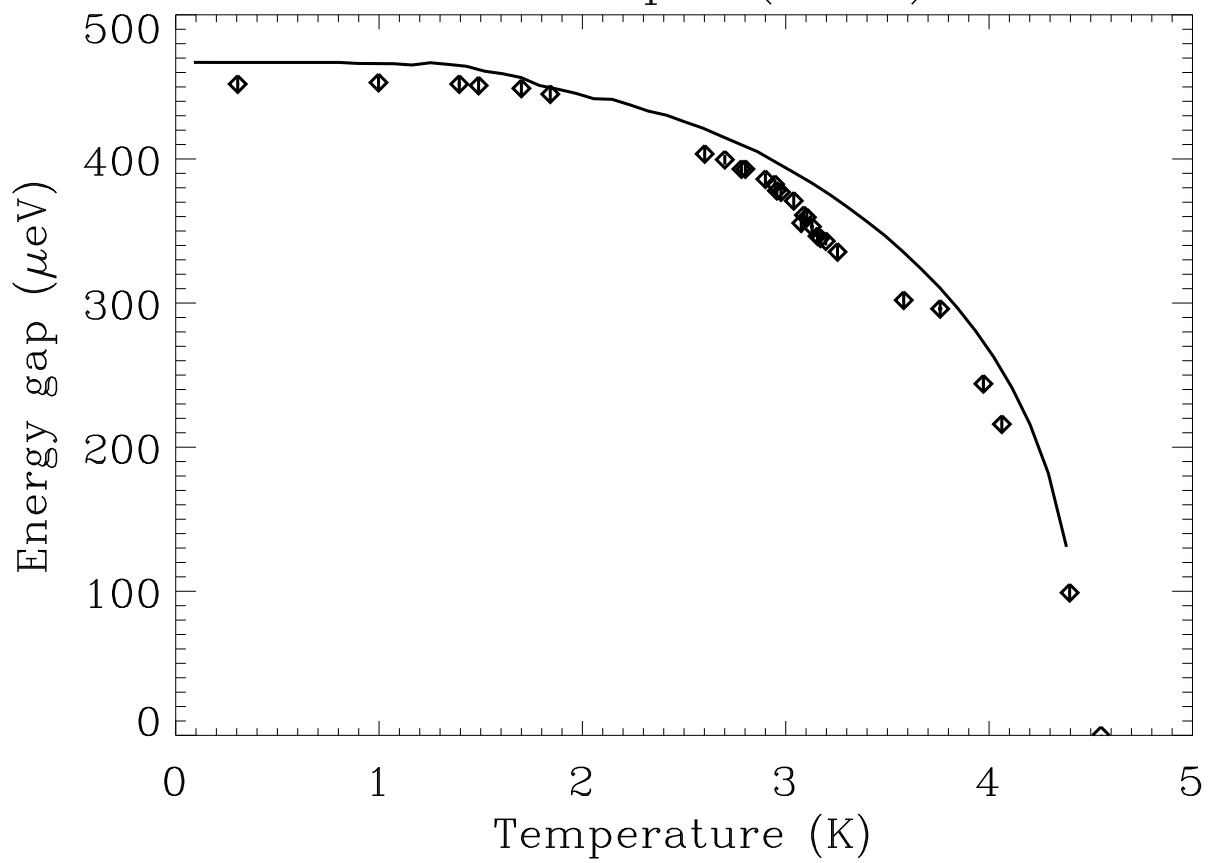
density of states for Al-Nb-Ta







Ta sample (Ta01)



Ta sample (Ta01)

